Journal of Magnetic Resonance 201 (2009) 186–198

Contents lists available at ScienceDirect

Journal of Magnetic Resonance

journal homepage: www.elsevier.com/locate/jmr

Image reconstructions with the rotating RF coil

A. Trakic *, H. Wang, E. Weber, B.K. Li, M. Poole, F. Liu, S. Crozier

The School of Information Technology and Electrical Engineering, The University of Queensland, Australia

ARTICLE INFO

Article history:
Received 16 July 2009
Revised 2 September 2009
Available online 11 September 2009

Keywords:
MRI
Rotating RF coil
RRFC
Coil sensitivity
TDM-SENSE
Coil coupling

ABSTRACT

Recent studies have shown that rotating a single RF transceive coil (RRFC) provides a uniform coverage of the object and brings a number of hardware advantages (i.e. requires only one RF channel, averts coil–coil coupling interactions and facilitates large-scale multi-nuclear imaging). Motion of the RF coil sensitivity profile however violates the standard Fourier Transform definition of a time-invariant signal, and the images reconstructed in this conventional manner can be degraded by ghosting artifacts. To overcome this problem, this paper presents Time Division Multiplexed — Sensitivity Encoding (TDM-SENSE), as a new image reconstruction scheme that exploits the rotation of the RF coil sensitivity profile to facilitate ghost-free image reconstructions and reductions in image acquisition time. A transceive RRFC system for head imaging at 2 Tesla was constructed and applied in a number of *in vivo* experiments. In this initial study, alias-free head images were obtained in half the usual scan time. It is hoped that new sequences and methods will be developed by taking advantage of coil motion.

© 2009 Elsevier Inc. All rights reserved.

1. Introduction

Partial Parallel Imaging (PPI) is an important innovation in MRI in the last decade [1–10]. In PPI, magnetic resonance (MR) signals are received simultaneously on multiple radio-frequency (RF) coils arranged in a phased-array like configuration and combined to obtain a full field-of-view (FOV) image. In such an array, each RF coil is characterized by unique coil sensitivity and provides an independent signal pathway. Parallel coil arrays are able to enhance the image quality or reduce the imaging time. In the Sensitivity Encoding (SENSE) approach for instance, Pruessmann et al. have shown that coil sensitivity profiles can be used as encoding functions complementary to Fourier preparation by magnetic field gradients [11–13]. SENSE accomplishes a reduction of scan time while yielding alias-free images. For increasing scan-time reduction factors (R) however, the number of RF coils L in the parallel array must be increased to satisfy a minimum number of encoding freedoms, which warrant an alias-free image reconstruction (i.e. $L \geqslant R$). However, increasing the number of RF coils invariably increases the electromagnetic coil coupling interactions, causing complex spatiotemporal RF field behavior and problems with the reconstruction process [14]. In addition, the number of coil channels increases, which further augments the complexity of the system and escalates fabrication costs. In practice, it can therefore be very difficult to engineer very large arrays [15–17].

Since increasing the number of coils to a very large number is extremely difficult, recent studies [18–20] have considered the generation of MR images by rapidly rotating a single RF transceive coil (RRFC). Although we have shown that the RRFC approach yields uniform and well-resolved images using only one RF transceive channel and averts mutual coil–coil coupling interactions, the studies did not describe how to optimally reconstruct images from the acquired k-space data.

In MRI, the object signal distribution is weighted by the RF coil sensitivity profile to produce the overall signal distribution. When reconstructing using the standard 2D — Inverse Fast Fourier Transform (2D-DIFFT), the overall signal distribution must be time-invariant. This is clearly not the case with the RRFC approach, as the sensitivity profile is changing spatially over time due to coil rotation. Therefore, in addition to gradient encoding, every k-space sample is additionally modulated both in amplitude and phase by a particular, complex sensitivity profile of the rotated RF coil. Effectively, an application of the 2D-DIFFT on the RRFC-acquired k-space is likely to introduce ghosting artifacts in the reconstructed image. For most 2D-DIFFT reconstructions, as we will see, the ghosting artifacts can be effectively displaced from the programmed field-of-view (FOV) by adjusting certain imaging parameters. Instead of relying on such parameter adjustments in practice, this paper introduces Time Division Multiplexed — Sensitivity Encoding, as one suitable image reconstruction scheme for standard and accelerated imaging with the RRFC. In essence, TDM-SENSE takes advantage of the RRFC sensitivity map to engender a

* Corresponding author. Address: Biomedical Engineering, The School of Information Technology and Electrical Engineering, The University of Queensland, 78 Staff House Road, St. Lucia 4072, Brisbane, Qld, Australia. Fax: +61 7 3365 4999.
E-mail address: trakic@itee.uq.edu.au (A. Trakic).

1090-7807/$ - see front matter © 2009 Elsevier Inc. All rights reserved.
doi:10.1016/j.jmr.2009.09.009

large number of encoding functions as useful complements to conventional gradient encoding.

2. Methods

2.1. General theory

Fig. 1a–b illustrates a single RF transceive coil that is free to rotate on a cylindrical surface about the object being imaged. When the RF coil is located at some initial angular position θ_0, it produces a complex spatial sensitivity map $s(\mathbf{r}_0)$, with $\mathbf{r}_0 = (x_0, y_0, z_0)^T$ as the spatial position vector defining the initial coordinates of the coil sensitivity.

When the RF coil is rotated about the imaged object at an angular frequency $\omega_c(t)$, a set of rotated sensitivity maps $s(\mathbf{r}, \theta_c(t))$ is produced at angles $\theta_c(t) = \int \omega_c(t)dt + \theta_0$ in a continuous time-sequential manner, with the following coordinate transformation:

$$(\mathbf{r}, \theta_c(t)) = R(\theta_c(t))\mathbf{r}_0 = \begin{pmatrix} \cos(\theta_c(t)) & \sin(\theta_c(t)) & 0 \\ -\sin(\theta_c(t)) & \cos(\theta_c(t)) & 0 \\ 0 & 0 & 1 \end{pmatrix} \begin{pmatrix} x_0 \\ y_0 \\ z_0 \end{pmatrix} \tag{1}$$

Although the RF coil can be rotated at a constant angular frequency, in a general system description, the angular frequency of the rotating RF coil is a function of time (i.e. $\omega_c(t)$). When the rotating RF transceive coil is used to excite the spin system, a complex RF transmission pulse $b_1(t)$ modulates $s(\mathbf{r}, \theta_c(t))$ to bring the initial net magnetization $m_0(\mathbf{r})$ towards the transverse plane:

$$m(\mathbf{r}) = i\gamma \int_0^{T_b} b_1(t)s(\mathbf{r}, \theta_c(t))m_0(\mathbf{r})e^{-2\pi i\mathbf{k}(t)\cdot\mathbf{r}}dt \tag{2}$$

$$\mathbf{k}(t) = \frac{\gamma}{2\pi} \int \mathbf{g}(\tau)d\tau \tag{3}$$

where $m(\mathbf{r})$ is the accumulated transverse magnetization distribution, $\mathbf{r} = (x, y, z)^T$ represents the spatial position vector, γ is the gyro-

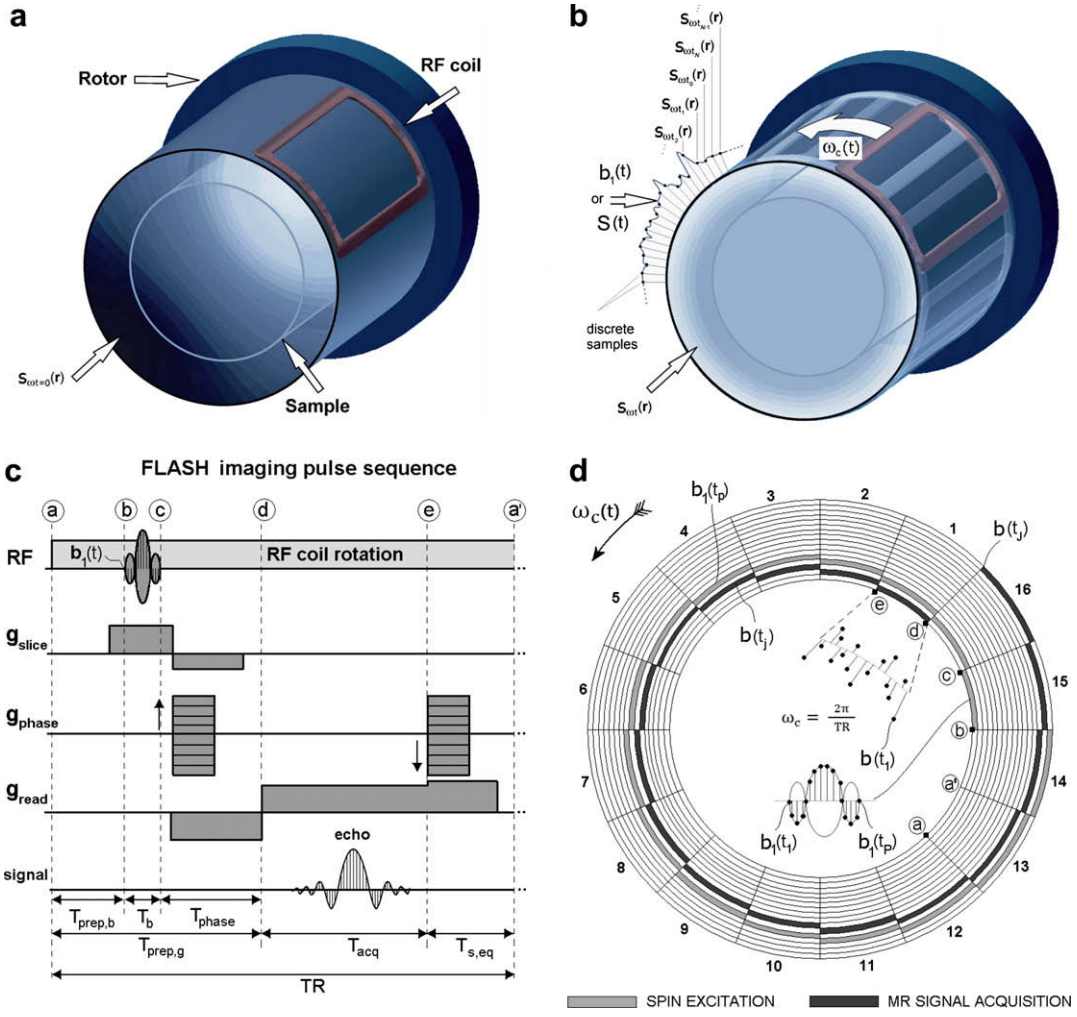

Fig. 1. (a) Illustration of a RF transceive coil attached to a rotor. The RF coil is stationary (i.e. $\omega_c(t) = 0$). (b) The RF coil is rotating around the imaged object at the angular frequency $\omega_c(t)$. As $b_1(t)$ is pulsed or $\mathbf{b}(t)$ is sampled, each discrete signal sample is weighted uniquely by the sensitivity profile $s(\mathbf{r}, \theta_c(t))$ produced by the RF coil. (c) The FLASH imaging pulse sequence. $T_{prep,b}$ and $T_{prep,g}$ are the preparation time periods for the RF transmission pulse and frequency encoding, T_{phase} is the time during which slice rephasing, phase encoding and frequency dephasing is performed, and $T_{s,eq}$ is the time period where frequency and phase dephasing is achieved followed by magnetization relaxation to the equilibrium state prior to the application of the subsequent pulse sequence for a new k-space line readout. Labels a, b, c, d, e and a′ are used to denote important points in time, that are referred to in (d). (d) Corresponding RRFC excitation and acquisition modes for an example 16×16 k-space. Illustrated are 16 circles, where each circle represents one full coil revolution and is equally discretized into 16 angular windows during which excitation and acquisition is performed. Each acquisition windows corresponds to one line in k-space. The numbers indicate the order of k-space lines, starting at 1 and ending at 16, while time stamps a, b, c, d, e and a′ correspond to those in (c). Each of the 16 data points per active window is weighted by a unique sensitivity map as the RF coil rotates at $\omega_c = 2\pi/TR$. Upon, the completion of 16 coil revolutions, entire k-space is acquired and the FOV uniformly covered.

magnetic ratio of the nuclear spin, T_b denotes the duration of the $b_1(t)$ pulse, $\mathbf{k}(t)$ is an arbitrary k-space trajectory obtained by pulsing magnetic field gradients $\mathbf{g} = (g_x, g_y, g_z)^T$, and τ is a dummy variable of integration. Eq. (2) is a generic form of spatially selective excitation of magnetization distribution $m_0(\mathbf{r})$ achieved by transmitting the RF pulse, $b_1(t)$, under guidance of the k-space trajectory, $\mathbf{k}(t)$.

Following the spin excitation, the rotating RF transceive coil can be used to receive the demodulated time-varying MR signal $b(t)$ that emanates from the spins in the object:

$$b(t) = \int_{-\infty(\mathbf{r})}^{\infty} s(\mathbf{r}, \theta_c(t)) m(\mathbf{r}, t) e^{-2\pi i \mathbf{k}(t)\cdot\mathbf{r}} d\mathbf{r} \tag{4}$$

$$m(\mathbf{r}, t) = m_0(\mathbf{r}) e^{-\frac{t}{T_2^*}} \left(1 - 2e^{-\frac{2TR-t}{2T_1}} + e^{-\frac{TR}{T_1}}\right) \tag{5}$$

where TR is the time of repetition, $m(\mathbf{r}, t)$ is the time-dependent magnetization at $\mathbf{r}$ for a gradient echo sequence, T_1 and T_2^* are the tissue-dependent longitudinal and transverse relaxation time constants as implicit functions of $\mathbf{r}$ and define the contrast in the image.

2.2. Time Division Multiplexed — Sensitivity Encoding (TDM-SENSE)

For a better understanding of the image acquisition with the RRFC, Eq. (2) and (4) can be written in discrete forms to comply with the digital instrumentation of the MRI system:

$$m(r_q) = i\gamma \sum_{p=1}^{P} b_1(t_p) s(r_q, \theta_c(t_p)) m_0(r_q) e^{-2\pi i k(t_p)\cdot r_q} \Delta t_{trans} \tag{6}$$

$$b(t_j) = \sum_{q=1}^{Q} s(r_q, \theta_c(t_j)) m(r_q) e^{-2\pi i k(t_j) r_q} \Delta t_{acq} \tag{7}$$

where Δt_{trans} and Δt_{acq} denote the dwell times in the digital transmit and receive chain, and P is the number of samples in $b_1(t)$. Eqs. (6) and (7) describe the formation of excited magnetization $m(r_q)$ and MR data sample $b(t_j)$ using discrete sampling in spatial, $\mathbf{r}_q(1\ldots Q)$, and temporal domain, ($t_j(1\ldots J)$, $t_p(1\ldots P)$), where p and j are indices in time, and q is an index in image space. Although Eqs. (6) and (7) describe a general three-dimensional case, to exemplify TDM-SENSE, we initially restrict the problem to two dimensions by assuming that an axial slice has been selected, so that $Q = N \times M$ and $J = U \times V$, where (N, M) and (U, V) are the discrete dimensions of the two-dimensional image and k-space. The entire sequence of spatial and k-space domain samples (Eqs. (6) and (7)) can be conveniently stored in measurement vectors, $m_{full} = (m(\mathrm{r}_1)\ldots m(r_Q))^T$ and $b_{full} = (b(t_1)\ldots b(t_J))^T$ so that the magnetization excitation and signal formation can be expressed in matrix forms:

$$\begin{pmatrix} m(r_1) \\ \vdots \\ m(r_Q) \end{pmatrix} = \begin{pmatrix} b_1(t_1) s(r_1, \theta_c(t_1)) e^{-2\pi i k(t_1) r_1} & \cdots & b_1(t_1) s(r_Q, \theta_c(t_1)) e^{-2\pi i k(t_1) r_Q} \\ \vdots & \ddots & \vdots \\ b_1(t_P) s(r_1, \theta_c(t_P)) e^{-2\pi i k(t_P) r_1} & \cdots & b_1(t_P) s(r_Q, \theta_c(t_P)) e^{-2\pi i k(t_P) r_Q} \end{pmatrix} \times \begin{pmatrix} m_0(r_1) \\ \vdots \\ m_0(r_Q) \end{pmatrix} = m_{full} = A m_{full,0} \tag{8}$$

$$\begin{pmatrix} b(t_1) \\ \vdots \\ b(t_J) \end{pmatrix} = \begin{pmatrix} s(r_1, \theta_c(t_1)) e^{-2\pi i k(t_1) r_1} & \cdots & s(r_Q, \theta_c(t_1)) e^{-2\pi i k(t_1) r_Q} \\ \vdots & \ddots & \vdots \\ s(r_1, \theta_c(t_J)) e^{-2\pi i k(t_J) r_1} & \cdots & s(r_Q, \theta_c(t_J)) e^{-2\pi i k(t_J) r_Q} \end{pmatrix} \times \begin{pmatrix} m(r_1) \\ \vdots \\ m(r_Q) \end{pmatrix} = b_{full} = B m_{full} \tag{9}$$

Substituting Eq. (8) in Eq. (9) gives:

$$b_{full} = A \cdot B m_{full,0} = E m_{full,0} \tag{10}$$

where $m_{full,0} = (m_0(r_1)\ldots m_0(r_Q))^T$ is the spatial signal distribution, representing the imaged object; $k(t_p) = [k_x(t_p), k_y(t_p)]^T|_{p=1\ldots P}$ and $k(t_j) = [k_x(t_j), k_y(t_j)]^T|_{j=1\ldots J}$ denote the k-space trajectories during transmission and reception. Image contrast is achieved in the usual manner of varying the time of echo (TE) and TR in the imaging experiment.

In Eqs. (8) and (9), A and B represent the excitation and encoding matrices, where every matrix element is weighted by a unique (complex) value of the rotated sensitivity map. Therefore, every element in b_{full} (i.e. k-space sample) is modulated by two rotated sensitivity profiles (i.e. one during RF pulse transmission and one during MR signal reception). Eq. (10) is a complete system description with E as the composite encoding matrix, which contains both transmission- and reception-type image encoding modulations (i.e. $E = A \cdot .B$, where '·' denotes the dot-product). While amplitude and phase scrambling of k-space data using RRFC is prone to introduce ghosting artifacts when the standard 2D-IFFT is applied to b_{full}, rotating the sensitivity profile while k-space samples are acquired provides additional, useful imaging encoding modulations that complement gradient encoding. Since rotating an RF coil about an object being imaged is emulating a parallel RF coil array in a time division multiplexing (TDM) fashion [21], the method outlined herein is accordingly named Time Division Multiplexed — Sensitivity Encoding (TDM-SENSE), and the system that implements the method, the rotating RF coil (RRFC).

To obtain a ghost-free image with TDM-SENSE, the RF coil sensitivity maps need to be known prior to image reconstruction. The operating system has now a trivial task of keeping a time-track of all the RF coil positions during both RF transmission and MR signal acquisition. With the knowledge of sensitivity profiles, the system matrix Eq. (10) is solved with $m_{full,0}$ as unknown. The most efficient way is to solve Eq. (10) iteratively using methods such as bi-conjugate gradient or least squares. In any case, the quality of the reconstructed image will, among others, depend on the condition of matrix E.

Although any imaging pulse sequence and gradient trajectory can in theory be used, to illustrate the underlying principles of TDM-SENSE, Fig. 1c shows a generic timing diagram of the gradient-recalled-echo-based Fast Low Flip Angle Shot (FLASH) imaging sequence [22], which was also used in the experiments of this study. Fig. 1d describes one example of spin excitation and MR signal acquisition using the RRFC with the FLASH imaging sequence. A series of excitation and acquisition modes similar to those illustrated in Fig. 1d can be achieved by varying the periods in the imaging sequence and $\omega_c(t)$ in a controlled manner.

2.3. Scan-time reduction with TDM-SENSE

Referring to MR signal acquisition Eq. (10), reducing the k-space trajectory by factor R along the phase encoding direction, while traversing the full k-space FOV, will result in the reduction of rows in B by the same factor (i.e. from J to J/R). Accordingly, the number of k-space samples for a $Q = N \times M$ image will be $J/R = U \times V/R$, and so the number of available basis functions may be insufficient to properly encode the image, resulting in an underdetermined system and in a reduced image quality once Eq. (11) is solved:

$$\begin{pmatrix} b(t_1) \\ \vdots \\ b(t_{J/R}) \end{pmatrix} = \begin{pmatrix} s(r_1, \theta_c(t_1)) e^{-2\pi i k(t_1) r_1} & \cdots & s(r_Q, \theta_c(t_1)) e^{-2\pi i k(t_1) r_Q} \\ \vdots & \ddots & \vdots \\ s(r_1, \theta_c(t_{J/R})) e^{-2\pi i k(t_J) r_1} & \cdots & s(r_Q, \theta_c(t_{J/R})) e^{-2\pi i k(t_{J/R}) r_Q} \end{pmatrix} \times \begin{pmatrix} m(r_1) \\ \vdots \\ m(r_Q) \end{pmatrix} \tag{11}$$

In order to maintain the full rank of B, the rotating RF coil has the potential to generate a new set of degrees of freedom that can substitute for the missing J/R rows in B. This can be accomplished by increasing the digital signal sampling rate by a factor of at least R, so that during a fixed acquisition time period Υ_{acq}, an R-fold increase in sensitivity maps will take place. In addition, increasing the rotational frequency of the RF coil increases the spatial separation among the coil sensitivities, yielding more distinguishable profiles and improved encoding properties. Upon solving the repopulated matrix system, the resulting MRI image should be free of aliasing artifacts. Fig. 2 illustrates an example of imaging time reduction with TDM-SENSE in the image acquisition stage. In this particular imaging sequence example, an increase in ω_c by at least a factor of R is mandatory in order to maintain a uniform coverage in the field-of-view (FOV) with the rotating RF coil (see Fig. 2d–f).

3. Experimental

3.1. Computer simulations

To assess the feasibility of TDM-SENSE, computer simulations were initially performed in Matlab (The Mathworks™) using the modified Shepp–Logan phantom. A hybrid Method-of-Moments/Finite-Element scheme [23] simulated the complex sensitivity map $s(\mathbf{r}_0)$ of a surface coil loop at 85.45 MHz. The computational problem was defined on an $N \times M = 80 \times 80$ test grid (FOV = 0.2 × 0.2 m) with the coil initially rotating at 18.8 rads^{-1}. The rotation of the sensitivity map was performed with the Matlab *imrotate* function, while for every incremental map rotation, $\pm 0.2\%$ of random noise was added to simulate the noise propagation. *k*-Space acquisition was based on the FLASH imaging protocol with TR = 500 ms, TE = 30 ms, T_b = 3 ms, $b_1(t)$ = gauss and f_{acq} = 10 kHz (with $\mathbf{k}(t) = 0$ in Eq. (6)). Eq. (10) was then solved using the Matlab in-built *lsqr* function. A series of accelerated TDM-SENSE simulations were performed by varying the reduction factor from $R = 1$ up to $R = 80$ and calculating the signal-to-noise ratio (SNR) in each case. The SNR was calculated by dividing the sum of image pixels in a small region of interest (7 × 7 pixels) within the Shepp–Logan phantom with one outside the phantom (7 × 7 pixels). The SNR was thereafter normalized (i.e. SNR_n) relative to the SNR result with $R = 1$. Since the SNR values are compared relative to each other, this particular approach of computing the SNR is valid. For absolute SNR measurements, more appropriate estimation protocols would be necessary. The TDM-SENSE simulation results can be seen in Fig. 4.

3.2. RRFC apparatus

A transceive RRFC system for head imaging at 2 Tesla, as shown in Fig. 3, was implemented to test the feasibility of imaging human anatomy with the rotating RF coil. The system was constructed mostly from plastic materials to be electromagnetically compatible with the MRI machine. A custom-designed pneumatic Tesla turbine [24] with ceramic bearings was used to rotate a transceive

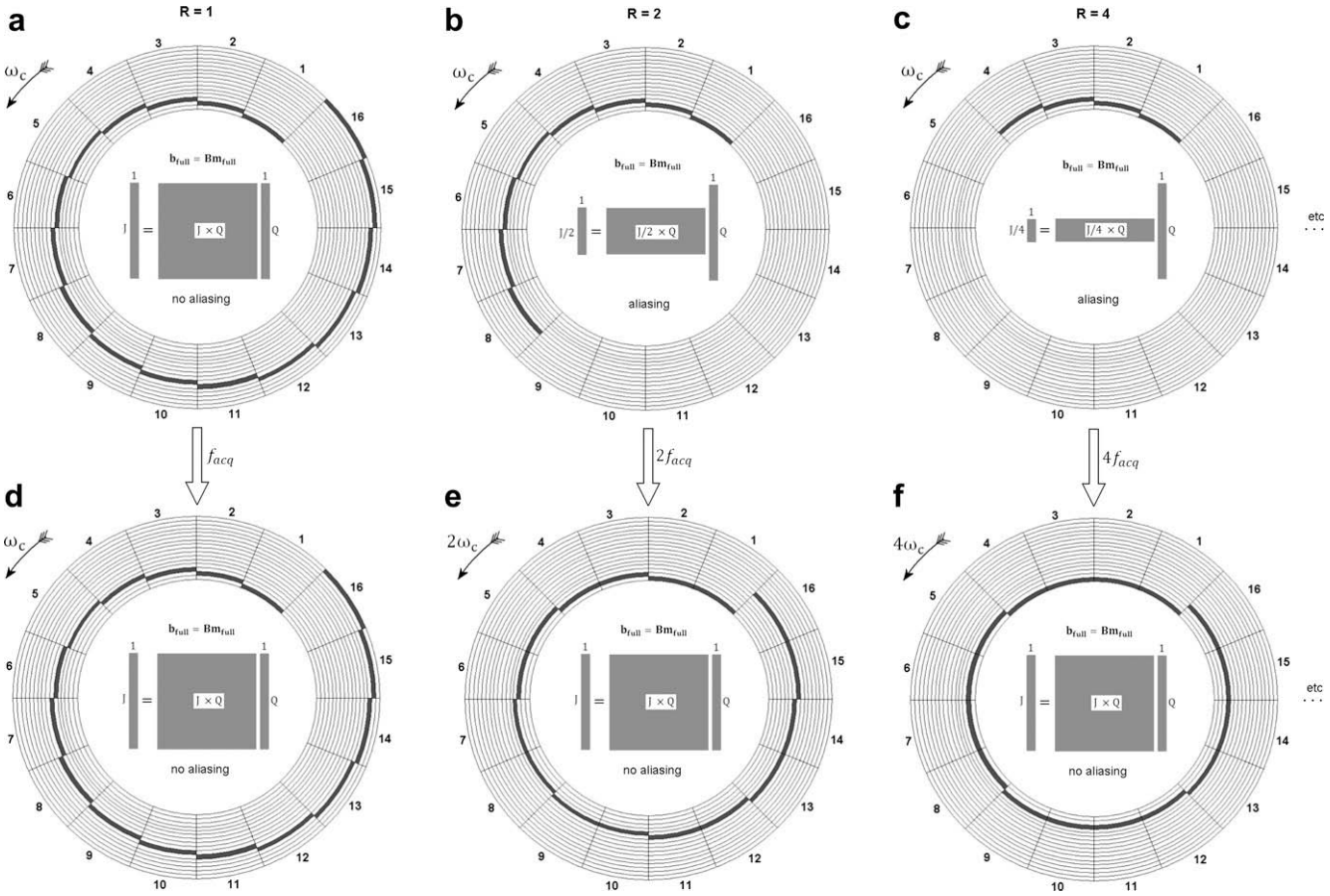

Fig. 2. Illustration of scan-time reduction based on RRFC acquisition example of Fig. 1d with constant ω_c. (a–c) shows the R-fold row reduction in the encoding matrix B and the corresponding reduction of phase encoding steps. Note that in this particular example, the FOV coverage diminishes with increasing reduction factor R. Images reconstructed from data in (a–c) would be degraded by aliasing artifacts. (d–f) Increasing f_{acq} and ω_c warrants a full size of B and a complete FOV coverage, respectively. In (e), only eight coil revolutions, rather than sixteen, are required.

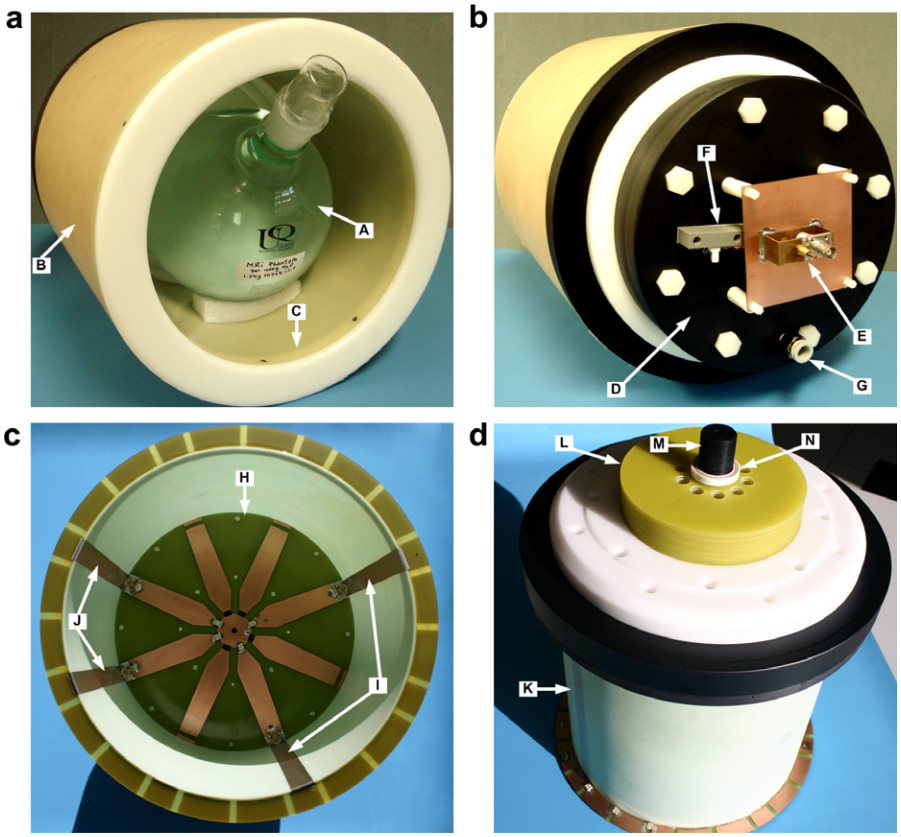

Fig. 3. (a) Front view of the rotating RF coil system designed for head imaging, measuring approximately 340 mm in diameter and 480 mm in length. The spherical solution phantom (A) is situated inside the system bore. The rotating RF transceive coil is residing between a slotted copper RF shield (not shown) situated on the inner side of the exterior cylinder (B) and object holding cylinder (C). (b) Rear view of the apparatus, showing Tesla turbine (D), the inductively-coupled RF link (E), infrared (IR) photo-interrupter (F) and pneumatic hose connector (G). (c) Front view of the rotating cylinder (K) and the engaged RF surface coil (I) that is connected to a printed circuit board (PCB) (H) situated at the end of the rotating cylinder. Label (J) indicates a smaller surface coil with spatially narrower sensitivity profile in angular direction, which we anticipate to use in future studies) (d) Side view of the assembly without the RF shield and the corresponding cylindrical cover. Shown are Tesla turbine discs (L), the end ceramic bearing (N) and rotating turbine shaft (M) after the turbine housing was taken off. The rotating cylinder (K) is also exposed.

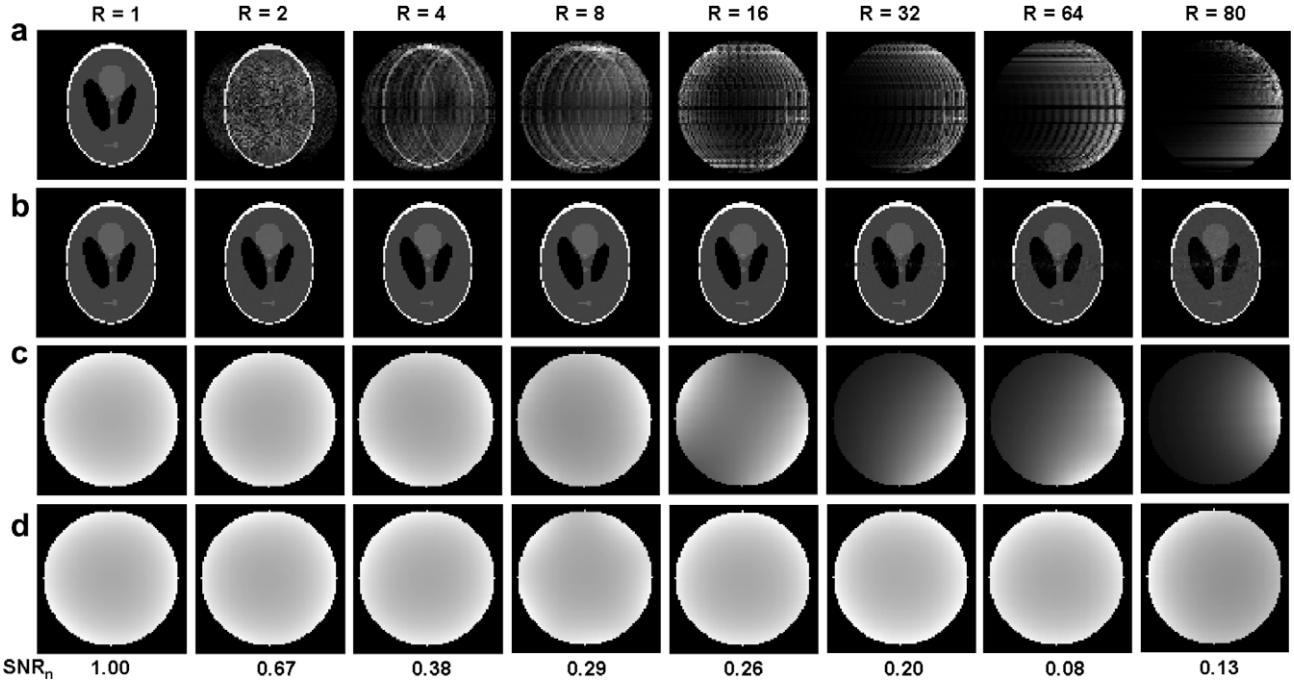

Fig. 4. TDM-SENSE simulation results with reduction factors ranging from $R = 1$ to $R = 80$ for an $N \times M = 80 \times 80$ image example. Reconstructed image of the Shepp–Logan phantom: (a) without and (b) with increasing f_{acq} and ω_c by the factor of R. The transceive field uniformity at the end of the imaging sequence: (c) without and (d) with increasing f_{acq} and ω_c by the factor of R. Subplots (b and d) indicate substantially lower image quality degradation due to Nyquist aliasing and good transceive uniformities at the end of the imaging sequence. In addition, normalized SNR values for each result in (b) are displayed, which indicate reasonable losses in SNR with substantially increasing R.

RF coil mounted on a light hollow cylinder, with an inner diameter of Ø = 280 mm, and a length of 300 mm. The Tesla turbine housed a total of fourteen Ø = 160 mm, 1.5 mm thick fibreglass discs separated by 0.8 mm, as shown in Fig. 3d. A prism shaped nozzle was machined into the Turbine housing and distributed air equally to all fourteen discs to achieve laminar flow. The transceive coil was a single surface coil loop that spanned a quarter periphery of the rotating cylinder (Fig. 3c). The coil loop was tuned and matched to 85.45 MHz and 50 Ohm input impedance under loaded conditions. A second, fixed concentric cylinder (Ø = 260 mm) with a plastic end-cap then acted as the sample/head holder, as Fig. 3a shows.

A Ø340 mm RF shield reduced power losses and a frictionless inductively-coupled RF link, resembling a RF transformer with one rotating (RF coil side) and one stationary (MR instrumentation side) assembly, connected the rotating RF coil to the MRI system. The inductive connector assembly was shielded to minimize power losses and noise perturbation. Compared to a standard RF coaxial connector, the inductive link suffered less than 1 dB power loss. The angular frequency of the rotating coil was governed by the air pressure drive to the Tesla turbine and measured with an infrared (IR) photo-interrupter. Overall, the air driving scheme constituted a regulated open-loop system and the maximum angular frequency was about 91.1 rads^{-1} (870 rpm) at a pressure of 35 psi after the apparatus was mechanically balanced. Full engineering details of the implemented prototype are outside the scope of this paper and will be provided in a subsequent publication.

3.3. Sensitivity profile estimation

Initially, all 2D-DIFFT image reconstructions were performed with the RRFC system in transceive configuration. TDM-SENSE requires however both the magnitudes and phases of the sensitivity maps corresponding to a large number of angular RF coil positions. Since it is impractical to measure a large number of sensitivities, we opted to estimate at least one map and rotate it numerically to engender many other profiles. Following the conventional approaches of sensitivity map extraction [11,25], we have initially removed the RF shield, reconfigured the RF coil for receive-only function and employed the body coil as a uniform transmitter and reference. Although removing of the RF shield augmented mutual coupling between the RRFC and the body coil, and substantially increased the amount of ghosting as result of modified system properties, the situation presented an opportunity to study the robustness of TDM-SENSE.

3.4. RRFC position measurement

To calculate the angular positions of the rotating receive-only RF coil and synchronize the positions with the events in the imaging pulse sequence, the square waveform signal from the IR photo-interrupter and the RF pulse gating signal from the spectrometer were simultaneously recorded on two separate channels of PowerLab/16SP (ADInstruments™, Model: ML795). The time between two consecutive RF gating signals was equivalent to the time of repetition (*TR*). Although the angular frequency of RRFC was changing by up to 2.4%-rms over several minutes due to periodic repressurising of the air compressor and due to the pneumatic open-loop driving configuration, it was assumed that the frequency of rotation was constant per a given *TR*. In addition, the rising edge of the square waveform was made to correspond to the position of the RF coil that produced the reference sensitivity map $s(\mathbf{r}_0)$. With the knowledge of the timing period between the RF gating pulse, the start and the end of the analog to digital conversion (ADC) of the MR signal, we were able to calculate the positions of the RF coil corresponding to the acquisition of the first and last sample of the discretized echo signal. Thereafter, the coil positions corresponding to the remaining N-2 and evenly spaced signal samples were assigned in a linear manner. One such waveform is shown in Fig. 9a.

3.5. Reconstruction

A computer program was written in C [26] to restructure the two-dimensional *k*-space data into the corresponding one-dimensional vector b_{full}, extract $s(\mathbf{r}_0)$ from the acquired images (see Fig. 8) and estimate the angular positions of the RF coil corresponding to the start and end of the MR signal acquisition. The elements in matrix E were then populated by rotating $s(\mathbf{r}_0)$ via complex plane rotation and spline interpolation routines and then multiplying the resulting values with the standard Fourier kernel (see Eqs. (8) and (9)). System Eq. (10) was solved iteratively using the least square QR factorisation method. During the reconstruction process, the computational region is defined by the thresholded image mask, similar to the conventional SENSE reconstruction [11]. Consequently, the resulting matrix *E* is rectangular, as it is reduced in size from the original number of columns $Q = N \times M$. This approach has proven to be quite effective in reducing the noise contribution in the resulting image [11]. The resulting one-dimensional vector $m_{full,0}$ was thereafter restructured into its corresponding two-dimensional form, which yielded the MR image free of ghosting artifacts.

4. Results

4.1. Computer simulations

Fig. 4a shows notable aliasing artifacts in reconstructed images when the number of phase encoding lines is evenly reduced by a factor of *R* while keeping all other parameters unaltered. In contrast, Fig. 4b shows alias-free images obtained by increasing the signal sampling rate f_{acq} and ω_c by *R*. According to the simulations, images without appreciable artifacts may be obtained, except for noise inhomogeneity visible at higher reduction factors. In addition, since the lost *k*-space data is continuously repopulated by increasing f_{acq} by *R*, the loss in SNR is not substantial at very high *R*. In contrast to Fig. 4c, and as predicted by the theory, Fig. 4d shows that in this particular combination of *TR* and ω_c, uniform transceive field uniformities can be obtained by also increasing ω_c by *R*.

4.2. 2D-DIFFT experiments

All imaging experiments were performed in a 2 Tesla whole-body MRI system (The University of Queensland, Australia) equipped with Bruker ParaVision 4.0 software. Head imaging was performed on a healthy 34 year old male volunteer under university guidelines. Throughout the experiments, the RRFC system was engaged in the transceive mode. MR images were reconstructed in the conventional 2D-DIFFT manner and therefore did not require a priori knowledge of RF coil positions and sensitivity profiles. Fig. 5a shows T_1 — weighted head images in all three planes when the RF coil is positioned to one side of the subject prior to spinning it. In this case, the RF coil can 'sense' only the region of the head that resides within the coil's field sensitivity distribution. In contrast, Fig. 5b shows complete head images when the RF transceive coil was rotating at a constant angular frequency of about 50.3 rads^{-1} (i.e. 480 rpm) while employing same imaging parameters as in Fig. 5a.

In another experiment involving a set of different imaging parameters (see legend of Fig. 5c), the RF coil was rotated at a constant speed of about 62.8 rads^{-1} (i.e. 600 rpm). The acquired

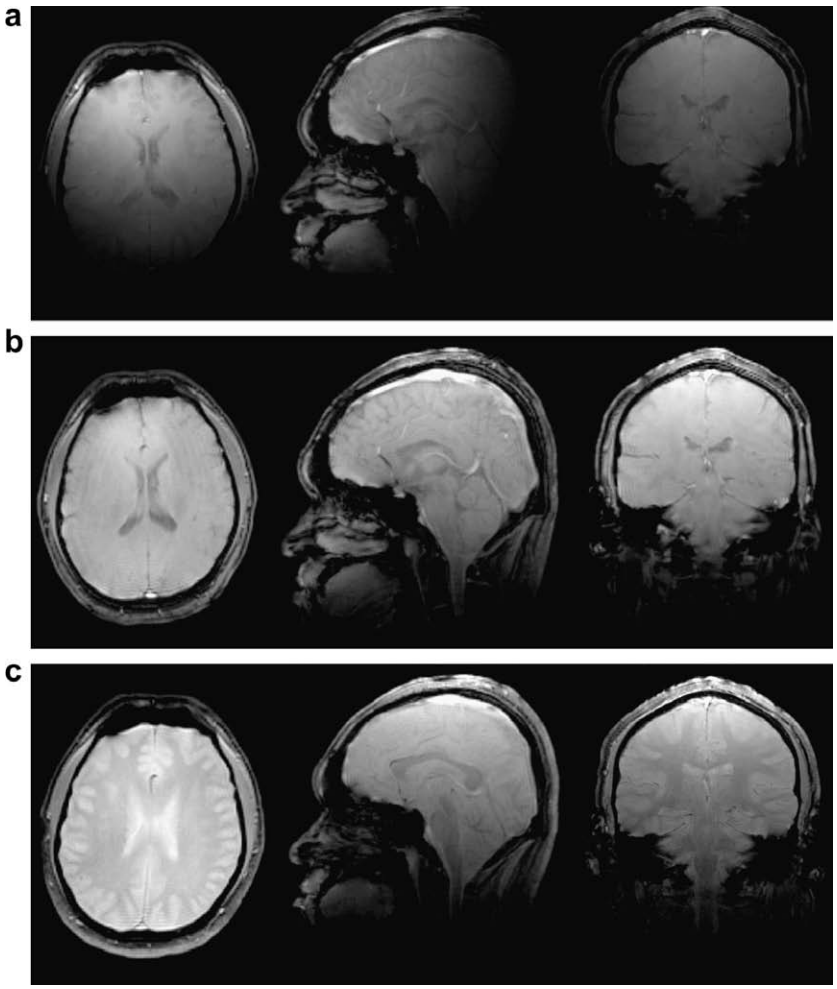

Fig. 5. 2D-DIFFT reconstructed head images in axial, coronal and sagittal plane obtained with the FLASH imaging sequence. Acquired T_1-weighted MR images when the RF transceive coil is: (a) stationary and (b) rotating at a constant angular frequency of 50.3 rads^{-1} (i.e. 480 rpm) relative to the subject's head. Following FLASH sequence imaging parameters were used: TR = 176 ms, TE = 7.25 ms, FOV = 30 × 30 cm, $N \times M$ =256 × 512, slice thickness (ST) = 5 mm, flip angle (FA) = 90°, $b_1(t)$ = gauss pulse, T_b = 3 ms, T_{acq} = 5.12 ms, f_{acq} = 50 kHz and R = 1. The images were acquired within 1 min 30 s. (c) Head images with the RF transceive coil rotating at 62.8 rads^{-1} while following FLASH imaging sequence parameters were used: TR = 158 ms, TE = 8.1 ms, FOV = 30 × 30 cm, $N \times M$ = 256 × 512, ST = 5 mm, FA = 45°, $b_1(t)$ = hermite pulse, T_b = 3.2 ms, T_{acq} = 5.12 ms, N_{ex} = 2, f_{acq} = 50 kHz and R = 1.

images, as shown in Fig. 5c, exemplify complete and well-resolved anatomical structures of the head. Image artifacts were precluded by averaging two experiments. These results show that rotating the coil at tens of rads^{-1} is adequate to achieve good tissue contrast at the given TR. Fig. 6 illustrates the effect of RF coil rotational frequency on the separation of ghosting artifacts. Specifically, Fig. 6a shows the ghosting artifacts in the image FOV due to sensitivity-based modulation of k-space data when the RF coil speed was set to a constant 35.8 rads^{-1}. In contrast, adjusting the speed of RF coil to about 44.5 rads^{-1} resulted in a complete ghost separation as shown in Fig. 6b. Alternatively, one could increase the FOV in y-direction, the number of averages or adjust the TR of the imaging sequence to achieve the same effect.

4.3. TDM-SENSE experiments

4.3.1. Sensitivity profile measurements

Fig. 7a shows axial head images obtained by fixing the rotating RF coil at eight angular positions interspaced by 45°. Each of the eight results was divided by a uniform brain reference to obtain raw sensitivity maps, which were refined afterwards by thresholding and polynomial fitting [11] to obtain smooth magnitude and phase profiles, as shown in Fig. 7b and c. The eight sensitivity maps were also polynomially fitted on a larger circular region and used to confirm that rotating any one of the maps would emulate the other seven sensitivity profiles.

4.3.2. Simulations based on experimental measurements

Simulations were initially performed to test TDM-SENSE in receive-only mode using the eight acquired head images and sensitivity profiles (Fig. 7a–c). It was assumed that the RF coil is rotating in such a way that the first echo signal was acquired from the first coil position, second echo from the second position, and so on, until in this case all 256 echoes (i.e. k-space lines) have been acquired in a total of 32 coil revolutions. Given the eight images from fixed coil locations, we assumed that the RF coil remained stationary during the acquisition of a k-space line, but was free to move relative to the phase encoding direction. Essentially, the k-space lines from the eight measurements were intermixed to create an effective b_{full} that imitated data acquired with the RF coil rotating in a hypothetical manner. Thereafter, matrix B was created using the extracted sensitivity profiles as shown in Fig. 7b and c. Fig. 7d is a comparison of image results (size: 256 × 256) after applying 2D-DIFFT and TDM-SENSE on the synthesized b_{full}. While

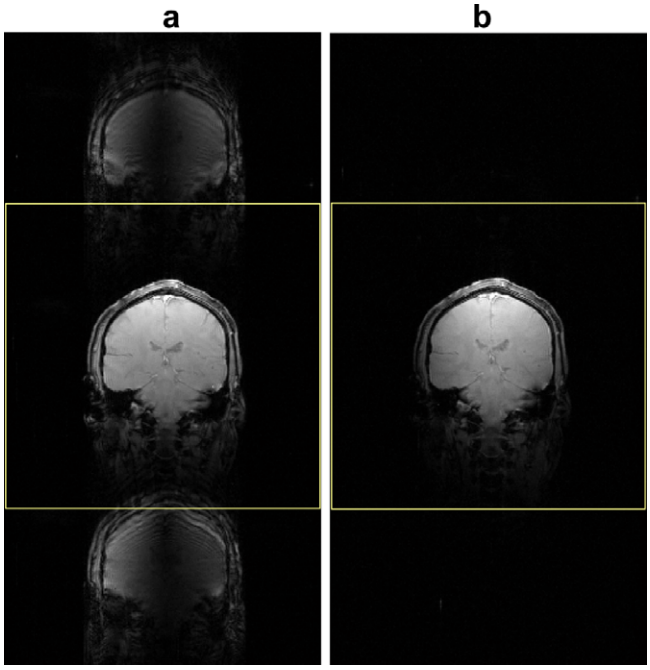

Fig. 6. An example of image ghost separation by adjusting the rotational frequency of the RF coil. Application of the 2D-DIFFT to the acquired 256×512 k-space yielded MR images, which were not cropped to the expected FOV. The bright box surrounding the central head image indicates the programmed FOV. The FLASH sequence parameters were as follows: TR = 156 ms, TE = 7.25 ms, FOV = 35×35 cm, $N \times M = 256 \times 512$, ST = 5 mm, $FA = 90°$, $b_1(t)$ = gauss pulse, T_b = 3 ms, T_{acq} = 5.12 ms, f_{acq} = 50 kHz and R = 1. (a) Image ghosting within the FOV obtained by rotating the RF coil at 35.8 rads^{-1}; and (b) The ghosts diverge from the image FOV when the coil is rotated at 44.5 rads^{-1}.

as expected, the 2D-DIFFT reconstructed image is notably affected by ghosting artifacts, TDM-SENSE provides a good quality and completely ghost-free image.

In a similar simulation, the eight acquired head images (size: 256×256) were also used to test the scan-time reduction of a 128×128 image. Following the theory of TDM-SENSE, every fourth k-space line was extracted from each of the eight acquired k-spaces (corresponding to images in Fig. 7a) in sequence (i.e. first line corresponding to first coil position, fourth line corresponding to second coil position, eight line from third position and so on). In this case, the size of the simulated k-space was 256×64, and according to TDM-SENSE, represented a scan-time reduction factor of $R = 2$ for a 128×128 image with a two-fold increase in f_{acq}. The resulting two-dimensional k-space (size: 256×64) was rewritten into a one-dimensional vector b_{full} (size: 1×16384). The encoding matrix B (size: $128^2 \times 128^2$) was populated with the measured sensitivity terms and gradient kernels. TDM-SENSE reconstruction was then performed by solving Eq. (10), while 2D-DIFFT was directly applied to b_{full} in two-dimensional form (size: 256×64). The results of TDM-SENSE and 2D-DIFFT reconstructions at $R = 2$ are displayed in Fig. 7e. While the 2D-DIFFT result is considerably degraded by aliasing artifacts in both spatial dimensions of the reduced FOV, the TDM-SENSE reconstructed image is of good quality, alias-free and covers the full-FOV.

4.3.3. Imaging experiment I

Fig. 8 is an example of a 128×128 image reconstruction with TDM-SENSE when the receive-only RF coil was rotating at about 9 rads^{-1}. The imaging parameters are detailed in the legend of Fig. 8. In particular, Fig. 8a is a plot of measured angular coil position as a function of the acquired k-space line number, and shows that from the start to end of one k-space line, the RF coil is displaced by only about 1.35°. We note that most sensitivity-based k-space weighting is along the phase encoding direction with minimal modulation along the frequency encoding direction. Fig. 8b is a distribution of all angular positions visited by the RF coil, which signifies a fairly uniform acquisition of the object signal distribution $m_{full,0}$. The results of image reconstruction with 2D-DIFFT and TDM-SENSE are shown in Fig. 9c and d. While in this particular receive-only configuration the 2D-DIFFT reconstructed image is substantially distorted, TDM-SENSE has reconstructed the image substantially free of ghosting artifacts. Considering that there is up to 15% of mutual coupling between the RRFC and the body coil, there are surprisingly only minute residual image artifacts in Fig. 9d. This finding suggests that MR images of much higher quality than presented here could be obtained with RRFC system in transceive configuration with the RF shield reinserted. This would avert present coil–coil coupling interactions completely and reemphasise the hardware advantages of the RRFC transceive approach.

4.3.4. Imaging experiment II

To reduce the scan time of a 128×128 image acquisition by a factor of two, the RF coil was set to rotate at a much higher angular frequency of about 82.8 rads^{-1}, while 512 samples were acquired per k-space line, with a total of 64 phase encodes. Fig. 9a is a plot of measured angular coil position versus the acquired k-space line number. In this case, during one line readout period of T_{acq} = 10.24 ms, the RF coil displaces an angular window of about 48.6°. If the RF coil were to rotate at a speed of 5859 rpm, it would complete one whole revolution during T_{acq}. Fig. 9b is a distribution of all angular positions visited by the RF coil at the start (outer circle) and at the end of signal acquisition (inner circle). Fig. 9c is the results of image reconstruction with 2D-DIFFT and shows notable aliasing artifacts within the reduced FOV. TDM-SENSE on the other hand has substantially minimized the energy of Nyquist aliases and provided a full-FOV image (see Fig. 9d). The remaining residual artifacts are most likely due to mutual coupling between the RF coil and body coil, which is spatially-invariant for different coil positions. To substantially reduce the residual artifacts, the spatially-invariant coupling interactions should be taken into account when $s(\mathbf{r}_0)$ is rotated to approximate other sensitivities. In Fig. 7d and e for instance, the image reconstructions are ideal, as coil coupling is inherent in the eight measured sensitivity profiles.

5. Discussion

In our recent publications [18–20], we have introduced and discussed the hardware advantages of rotating a single RF transceive coil to emulate stationary RF coil arrays. In this study, MRI with the RRFC system has been performed in combination with TDM-SENSE. The numerical and experimental results support the underlying theory of TDM-SENSE as a means of alias-free image reconstruction. A two-fold scan-time reduction was accomplished by increasing the signal sampling rate and the angular frequency of coil rotation. The following paragraphs discuss the advantages and disadvantages of TDM-SENSE on the RRFC platform.

5.1. On the image reconstruction

While the premise of RRFC is to gain certain hardware advantages over parallel RF coil arrays, the approach violates the time-invariant signal definition of the (Fast) Fourier Transform. TDM-SENSE has therefore been implemented as a more suitable and generic method of reconstructing ghost-free images. With TDM-SENSE, k-space data points are sampled in the usual time-sequential manner, where every k-space sample is uniquely modulated by a rotated sensitivity map, which itself is a function of time. In this

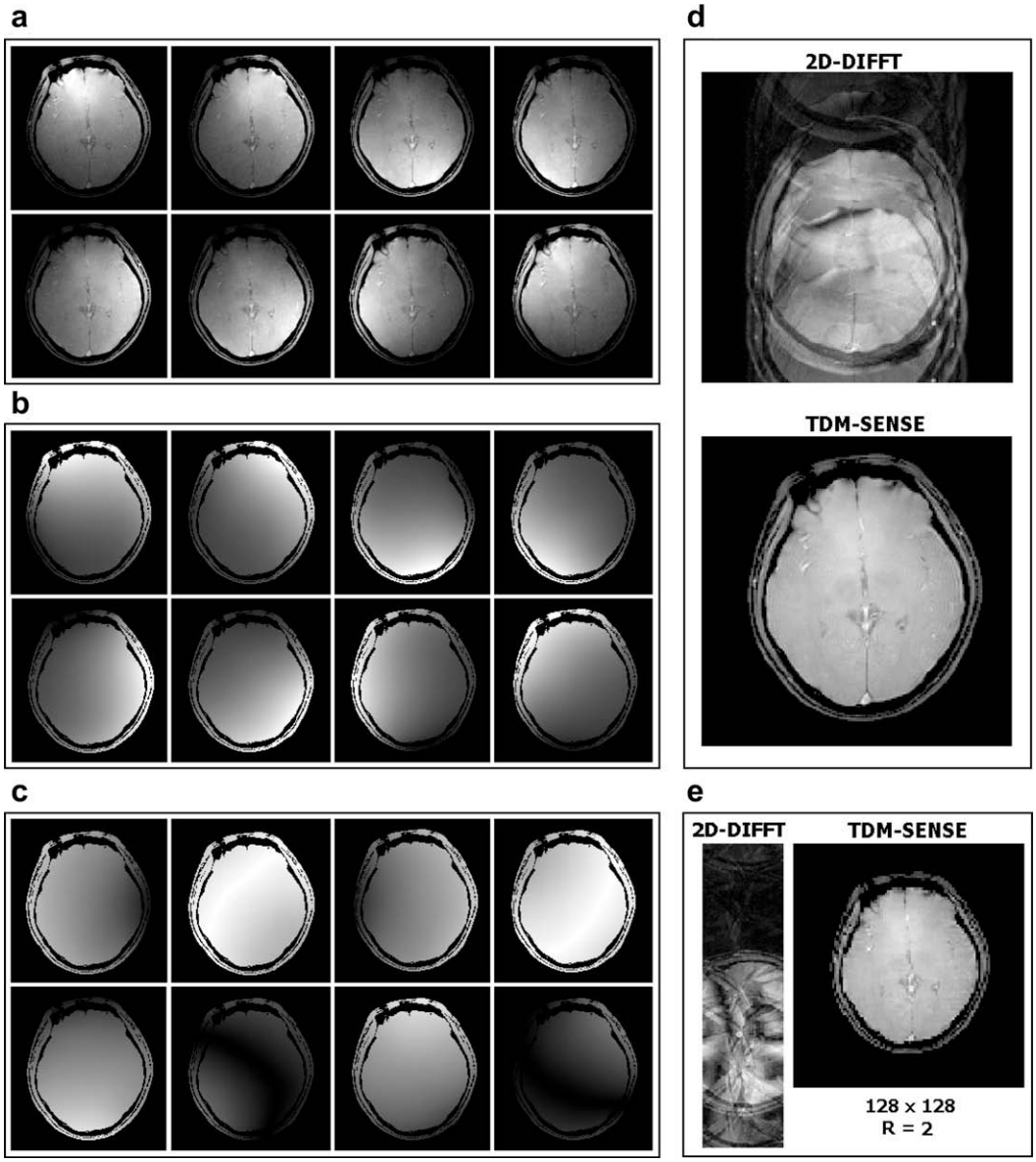

Fig. 7. (a) Raw axial head images acquired with the RF coil fixed at eight positions with an equal angular interspacing of 45°. Following FLASH imaging sequence parameters were used: $TR = 100$ ms, $TE = 8.19$ ms, FOV = 35 × 35 cm, N × M = 256 × 256, $ST = 5$ mm, $FA = 30°$, $b_1(t)$ = hermite pulse, $T_b = 3$ ms, $T_{acq} = 5.12$ ms, $T_{prep,b} = 2.1$ ms, $T_{prep,g} = 15.3$ ms, $N_{ex} = 1$, $f_{acq} = 50$ kHz and $R = 1$. (b and c) show polynomially fitted and thresholded magnitude and phase plots of the RF coil obtained by dividing each raw measurement in (a) by the uniform brain reference. (d) 2D-DIFFT and TDM-SENSE reconstructed 256 × 256 image at $R = 1$ based on the synthesized b_{full}. (e) 2D-DIFFT and TDM-SENSE reconstructed 128 × 128 image at $R = 2$ based on the synthesized b_{full} (see text for more information).

way, the sensitivity coefficients are exclusively coupled to the Fourier kernels in Eqs. (8) and (9) and contribute as additional image encoding functions. Solving Eq. (10) can be numerically challenging, as with the increasing image size, the encoding matrix E becomes comprehensively large (i.e. $N^2 \times M^2$). One possibility to alleviate this computational burden is to parallelize Eq. (10) on a computer cluster and then solve the problem iteratively [27].

5.2. On other suitable schemes

Based on the generic form of Eq. (10), TDM-SENSE should apply equally well to other imaging pulse sequence and modes of k-space traversal. Due to their rotational periodicity, pulse sequences that employ k-space trajectories such as spirals, rosettes and circles would be quite suitable to RRFC in that all the underlying system equations are expressible in polar coordinates. For optimal performance, there may however be a requirement to synchronize the k-space trajectory with the rotation of the RF coil sensitivity map. Presently, reconstruction from non-Cartesian sampling patterns is often inconvenient on many MRI installations that rely heavily on Cartesian coordinates. Recent years have seen a notable increase in the development of polar reconstruction methods such as the Polar Fourier Transform (PFT) [28], k-space regridding and interpolation techniques [29], which should render regular use of non-Cartesian k-space trajectories practical in the future. Single shot sequences such as the Echo Planar Imaging (EPI) sequence conform well to the serial acquisition nature of RRFC in that the entire k-space can be acquired in one or more complete coil revolutions. The RRFC approach could be useful in RF encoding applications (i.e. Rotating Frame Zeugmatography), where a series of RF pulses is applied without gradient switching to encode the spatial information [30]. It is bourn in mind that a series of new

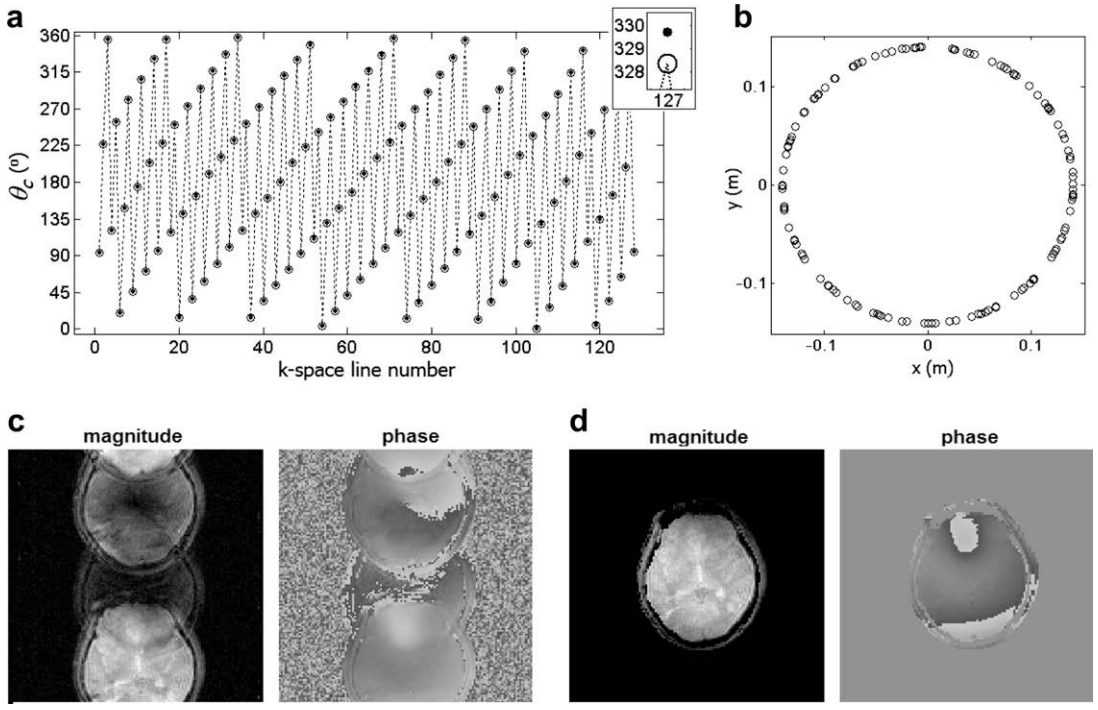

Fig. 8. Comparison of 2D-DIFFT and TDM-SENSE image reconstruction with $R = 1$. Following FLASH imaging sequence parameters were used: $TR = 100$ ms, $TE = 8.19$ ms, FOV = 35 × 35 cm, $N \times M = 128 \times 128$, $ST = 5$ mm, $FA = 30°$, $b_1(t)$ = hermite pulse, $T_b = 3$ ms, $T_{acq} = 2.56$ ms, $T_{prep,b} = 2.1$ ms, $T_{prep,g} = 10.3$ ms, $N_{ex} = 1$, $f_{acq} = 50$ kHz and $R = 1$. (a) Measured angular coil positions when the RF coil was rotating at about 9 rads^{-1}. (b) Distributions of all angular positions visited by the rotating RF coil. (c and d) 2D-DIFFT (spectrometer) and TDM-SENSE reconstructed brain image, respectively.

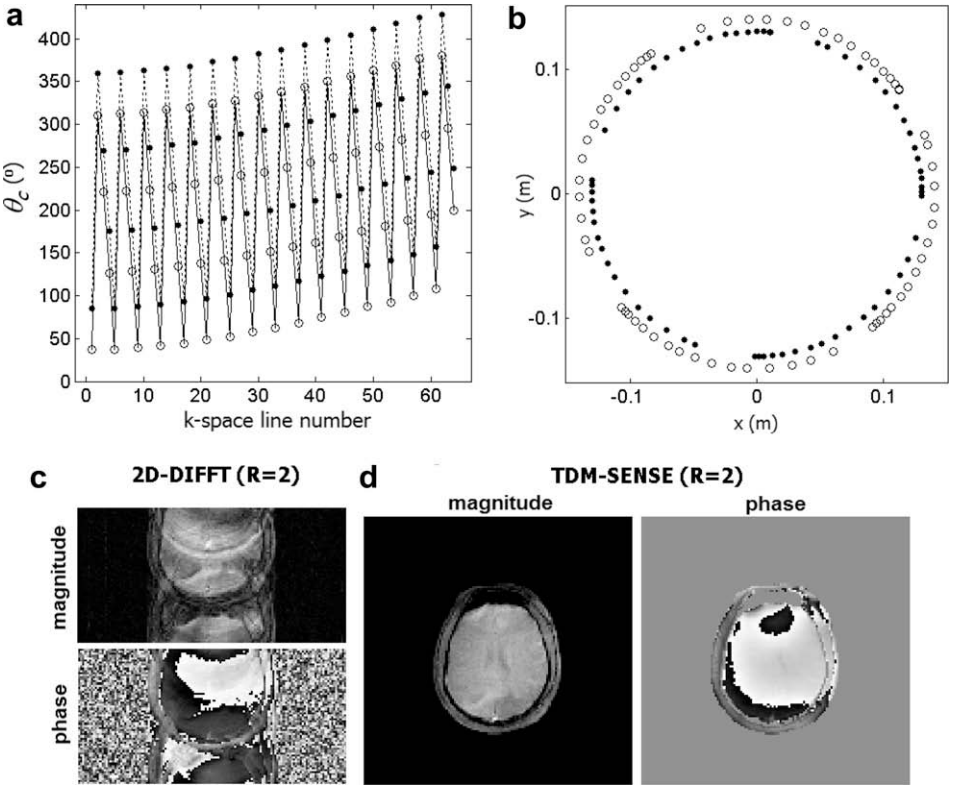

Fig. 9. Comparison of 2D-DIFFT and TDM-SENSE 128 × 128 image reconstruction with $R = 2$. Following FLASH imaging sequence parameters were used: $TR = 100$ ms, $TE = 10.16$ ms, FOV = 35 × 35 cm, 512 frequency and 64 phase readouts, $ST = 5$ mm, $FA = 30°$, $b_1(t)$ = hermite pulse, $T_b = 3$ ms, $T_{acq} = 10.24$ ms, $T_{prep,b} = 2.1$ ms, $T_{prep,g} = 10.97$ ms, $N_{ex} = 1$, $f_{acq} = 50$ kHz. (a) Measured angular coil positions when the RF coil was rotating at about 82.8 rads^{-1}, where circles and dots indicate start and end of the signal acquisition; (b) distribution of angular positions visited by the RF coil (according to measurements in (b)); (c and d) show magnitude and phase plots of the 2D-DIFFT and TDM-SENSE reconstructed brain image, respectively.

pulse sequences and methods can be developed by taking advantage of coil rotation. The particular advantages and disadvantages of these schemes are beyond the scope of this paper and shall be investigated in future studies.

5.3. On the RF coil sensitivity

TDM-SENSE requires sensitivity maps corresponding to an extremely large number of angular RF coil positions. In practice, it is infeasible to measure all the required sensitivity profiles. Instead, one or fewer sensitivity maps can be estimated and thereafter numerically rotated to engender many other sensitivity profiles as required. This is a valid approach for most low field applications, in that the spatial RF field distribution is insignificantly affected by the imaged object as the dielectric load. Evidently, more sophisticated sensitivity estimation protocols will be required if TDM-SENSE is to be used at higher fields where the sensitivity profiles are notably and non-uniformly distorted by field/tissue interactions. With increasing R, TDM-SENSE relies heavily on the accuracy and property of the rotating sensitivity map. In other words, the image SNR decreases with increasing R, which is to be expected with SENSE-based implementations. Theoretically, increasing the image SNR could be accomplished by narrowing the frequency domain representation of the RF coil sensitivity profile in the angular direction. The sensitivity profile may then be considered as a spatial filter with a narrow bandwidth that receives nearby signals with good SNR and attenuates the noise from the regions where the amplitude of coil sensitivity diminishes.

5.4. On practical considerations

There are a number of important considerations relating to the design of an RRFC system. Presently, the constructed RRFC head imaging system is able to achieve rotational speeds of 870 rpm. For further scan-time reduction with TDM-SENSE, it is desirable to rotate the RF coil at higher angular frequencies in order to further separate the sensitivity maps and also to increase the sampling rate on the spectrometer. In practice, rotational speeds of up to 150,000 rpm are achievable using air turbines that employ ceramic bearings [31] while the MHz-range clock frequencies are already available with commercial ADCs and modern MRI spectrometers. Higher rotational speeds could find applications with small rotating RF coils, which are not expected to exhibit strong mechanical vibrations and large angular moments. Another important design consideration relates to the accurate control of RF coil position and speed. Precision control can for instance be achieved by interfacing the MRI instrumentation to a feedback-circuit controller at the RRFC system end. These and other considerations are currently work in progress.

5.5. Qualitative comparison of SNR in PCA and RRFC

The signal-to-noise (SNR) ratio is an important parameter for quantifying image quality in MRI. The image reconstruction and SNR of a parallel coil array (PCA) have been reviewed in the Appendix. In the following, we qualitatively compare RRFC with PCA in terms of SNR.

RRFC emulation: Theoretically, it is possible to extend the PCA Eqs. (A1), (A2), (A3), (A4), (A5) to the RRFC approach by assuming a massively parallel coil array consisting of $L = J$ evenly distributed coils, where J is total number of acquired k-space samples. To emulate time-division-multiplexing of RRFC on such a large array, it is assumed that any jth k-space sample is acquired only with the lth RF coil, with all other coils absent. There are two important consequences of this model. First, all $l \neq j$ terms in $\mathbf{b}$ and $\mathbf{B}$ become zero (i.e. $B_{(lj),q} = 0$ and $b_l(\mathbf{k}_j) = 0$, for $l \neq j$). This effectively reduces the number of rows in Eq. (A2) from $LJ = J^2$ to $L = J$. The encoding matrix $\mathbf{B}$ is reduced to: $B_{l,q} = s_l(\mathbf{r}_q)e^{-2\pi i(\mathbf{k}_l \cdot \mathbf{r}_q)}$. Second, all off-diagonal terms in noise covariance matrix $\mathbf{\Psi}$ vanish in the absence of inductive coil coupling (i.e. correlation terms are zero: $\mathbf{\Psi}_{l,l'} = 0$, for $l \neq l'$). This implies that there is no overlapping of electric field $\mathbf{E}(\mathbf{r})$ patterns, and for RRFC, Eq. (A4) simplifies to:

$$\mathbf{\Psi}_{l,l} \equiv \int \sigma(\mathbf{r})|\mathbf{E}_l|^2(\mathbf{r})d^3\mathbf{r} \tag{12}$$

Therefore according to Eq. (A5), for a scan-time reduction factor $R = 1$ and fixed sampling rate f_{acq}, a PCA consisting of L independent channels acquires L-times more k-space samples n_k than the RRFC system. Assuming that the L coils in the parallel array are completely decoupled, the image SNR of a parallel array would in this case be $\sqrt{L}$ times higher than the SNR of RRFC. In practice however, this ideal $\sqrt{L}$ SNR gain is almost impossible to attain due to increased inductive and resistive losses in the array, as is discussed in the subsequent paragraphs. Considering RRFC, one way to increase n_k and engender additional rows in Eq. (A2), is to increase the signal sampling rate f_{acq} by factor L. Provided that the receiver bandwidth Δf is unaltered, according to Eq. (A5) (Appendix), this increase would at best result in a $\sqrt{L}$ improvement in SNR. The results in this study (Figs. 4, 7–9) suggest that improved image encoding properties are attained by keeping the number of rows in Eq. (A2) (i.e. k-space samples) larger or equal to the number of columns (i.e. image pixels), in particular as the scan-time reduction factor R is increased. Similarly, we could increase the sampling rate on the parallel array to engender additional k-space samples, however, the situation may differ somewhat. While a rotating RF coil is capable of weighting each new acquired k-space sample differently, any stationary element in the parallel array weights the additional samples with the same sensitivity profile. Therefore, in the PCA, the elements of the encoding matrix $\mathbf{B}$ would differ only by the magnetization phase that is incurred through switching field gradients over time. In the case of RRFC, the variance among element in matrix $\mathbf{B}$ could be optimized by tailoring the coil sensitivity profile and the speed of rotation. Further investigations are required to quantify the SNR performance of the RRFC system and compare it in an appropriate manner with the SNR of different parallel array configurations.

Inductive and resistive losses: The common approach to increase SNR or equivalently reduce the scan time, is to employ a larger number coils in the parallel array. While this trend incurs additional manufacturing costs due to the added electronics channels, it also creates a series of design issues relating to increased inductive and resistive losses.

When array coils couple inductively, they tend to resonate as a single structure, and it can be very difficult to simultaneously match the impedance of each element to the input impedance of the corresponding receiver unit. This non-optimal impedance match degrades the pre-amplifier noise figure and effectively the resulting image SNR. Partially parallel reconstruction schemes, such as SENSE, require distinct component-coil sensitivity profiles to appropriately encode the spatial information [11]. As array coils couple inductively, they become sensitive to the same regions of the sample, thus diminishing the distinctiveness among component sensitivity patterns. Overlapping RF coils to reduce the shared magnetic flux imposes stringent limitations on the placement of coil elements [3]. Lumped decoupling networks [32] and low input impedance pre-amplifiers [3,33] are now routine techniques for decoupling arbitrarily arranged arrays. Such techniques perform reasonably well with modest receive-only arrays, where up to ~30 dB of decoupling (i.e. ~3% cross-talk) is attainable. Unfortunately, there is still no accepted optimal method for decoupling transceive arrays [32]. Just as inductively coupled coils share signal voltages, they also share noise voltages in the same proportion.

Therefore, depending on the PCA design, noise received by coupled coils can exhibit a high degree of correlation (i.e. large off-diagonal elements in $\mathbf{\Psi}$). For instance, noise correlations of up to 43% and 53% were reported in practice with 12-channel and 96-channel PCAs for head imaging [34]. These and other findings [2,6,15–17] suggest that, extending the routine decoupling techniques to large numbers of coils with varying amounts of shared inductance is quite complex and challenging. Other PCA engineering issues relate to the optimal loop size and increased resistive losses [35]. For instance, in order to accommodate a larger array on a prescribed geometry, one must often resort to smaller coil loops. Although small loops offer better SNR for nearby target regions, they exhibit poorer RF field penetration and therefore lower SNR in distal tissue regions. As the loop size decreases, coil noise increases relative to the sample noise, deeming smaller coils less efficient than larger coils. Likewise, the number of pre-amplifiers, cables, lumped capacitive/inductive components and solder joints increases in proportion to the number of added array coils. This trend ultimately leads to a substantially larger $R_{conductor}$, therefore R_{tot}, and the noise power increases in direct proportion to R_{tot}, thus reducing the overall SNR (Eq. (A5), Appendix). A similar issue arises from the perspective of the sample noise, R_{sample}. When the electric fields of various coil sensitivities are overlapped within an array (Eq. (A4), Appendix), sample noise becomes correlated. The amount of correlation depends on the level and nature of the electric field overlap. This effectively places stringent constraints on how the coils are positioned in the array.

In the case of the RRFC system however, the situation is different. Since there is only one RF coil that moves relative to the sample, there are no inductive coil-to-coil coupling interactions, and the sample R_{sample} and system resistances $R_{conductor}$ are minimal (i.e. no overlapping of electric fields, and there are only one coil, one pre-amplifier, one coaxial cable and fewer lumped components and solder connections). Therefore, the overall noise voltage v_n is expected to be much smaller than that of a PCA. In addition, RRFC offers much more freedom in choosing the optimal coil loop size and shape as function of SNR, field penetration and encoding properties. Although RRFC demonstrates sensitivity-based image encoding and scan-time reduction capabilities, given the identical signal sampling rates, it fails to match the overall SNR performance of the PCA. Since RRFC is not limited to only one rotating RF coil, in the scope of spatial encoding and SNR, it would be worth investigating the benefits of hybridizing PCA and RRFC systems.

6. Conclusions

This paper has introduced TDM-SENSE as one suitable alias-free image reconstruction scheme dedicated to the RRFC system. With TDM-SENSE, the time-sequential generation of rotated sensitivity maps corresponds to an increase in encoding degrees of freedom. A RRFC system for head imaging at 2 Tesla was implemented and evaluated in a number of *in vivo* experiments. In this initial study, two-fold scan-time reduction was achieved with TDM-SENSE by increasing the signal sampling rate and the angular frequency of coil rotation. Our future efforts will involve the development of more optimal methods for dispensing phase encoding steps by taking advantage of the numerous sensitivities generated by the RRFC.

Acknowledgments

Financial support from the Australian Research Council is gratefully acknowledged.

Appendix

For the purposes of image reconstruction with a parallel coil array (PCA), the MR signal received by the lth coil in an array of L coils at k-space point $\mathbf{k}_j$ due to a distribution of transverse magnetization $m(\mathbf{r})$ is discretized and written in the form:

$$b_l(\mathbf{k}_j) \approx \sum_{q=1}^{Q} s_l(\mathbf{r}_q) m(\mathbf{r}_q) e^{-2\pi i(\mathbf{k}_j \cdot \mathbf{r}_q)} + n_l(\mathbf{k}_j) \tag{A1}$$

where $s_l(\mathbf{r}_q)$ is the complex sensitivity map of coil l and $n_l(\mathbf{k}_j) \equiv n_l$ is the time-dependent Gaussian random variable representing white noise. While the noise received by several RF coils in parallel is usually correlated, the noise accompanying each point in k-space is statistically independent. For each coil $l = 1 \ldots L$, we can write a matrix equation in the form $\mathbf{b}_l = \mathbf{B}_l\ \mathbf{m} + \mathbf{n}_l$, where $B_{(lj),q} = s_l(\mathbf{r}_q) e^{-2\pi i(\mathbf{k}_l \cdot \mathbf{r}_q)}$. Stacking all the coil signal vectors $\mathbf{b}_l$ into a single column vector $\mathbf{b}$, we obtain a complete matrix representation of the signal received by the PCA:

$$\begin{pmatrix} \mathbf{b}_1 \\ \mathbf{b}_2 \\ \vdots \\ \mathbf{b}_L \end{pmatrix} = \begin{pmatrix} \mathbf{B}_1 \\ \mathbf{B}_2 \\ \vdots \\ \mathbf{B}_L \end{pmatrix} \mathbf{m} + \begin{pmatrix} \mathbf{n}_1(t) \\ \mathbf{n}_2(t) \\ \vdots \\ \mathbf{n}_L(t) \end{pmatrix} \equiv \mathbf{b} = \mathbf{B}\mathbf{m} + \mathbf{n}(t) \tag{A2}$$

Eq. (A2) can be solved using modified Moore–Penrose pseudo-inverse to yield a minimum norm matrix inverse [11]:

$$\mathbf{B}^{inverse} = \mathbf{X}\mathbf{B}^H \mathbf{\Psi}^{-1} \quad \text{with} \quad \mathbf{X} = \frac{1}{n_k} (\mathbf{B}^H \mathbf{\Psi}^{-1} \mathbf{B})^{-1} \tag{A3}$$

where n_k the total number of acquired k-space samples (here $n_k = JL = \text{length}(\mathbf{b})$) and $\mathbf{\Psi}$ is the noise covariance matrix, which includes the noise received by individual coils as well as the amount of correlated noise that exists between each pair of coils. Incidentally, the noise covariance matrix represents the overlap of the electric fields $\mathbf{E}_l(\mathbf{r})$ among different sensitivity patterns within the PCA [3]:

$$\mathbf{\Psi}_{l,l'} \equiv \int \sigma(\mathbf{r}) \mathbf{E}_l(\mathbf{r}) \cdot \mathbf{E}^*_{l'}(\mathbf{r})\, d^3\mathbf{r} \tag{A4}$$

where $\sigma(\mathbf{r})$ is the conductivity of the sample being imaged. To evaluate the SNR of a RF system, various sources of signal and noise must be taken into consideration. The SNR is commonly written as: $\text{SNR} = v_{sig}^2 / v_n^2$, where v_{sig} and v_n are the overall signal and noise voltages.

For a RF system, it can then be shown that [38]:

$$\text{SNR} \propto \frac{m_0 \mu(\mathbf{r}) \omega \sqrt{n_k}}{\sqrt{4 k_B T \Delta f\ R_{tot}}} \tag{A5}$$

where m_0 the spin magnetization, $\mu(\mathbf{r})$ the magnetic permeability of the sample, ω the Larmor frequency, k_B the Boltzmann constant, T the absolute temperature, Δf the receiver bandwidth and R_{tot} the overall resistance seen at the output terminals of the RF system. In our analysis, we will be particularly interested in variables n_k and R_{tot}, as these differ between PCA and RRFC.Among the various mechanisms that underlie noise in MR detection, resistive losses in the sample and coil are considered as the two major sources of noise [3]. Sample noise results from thermal agitation of charged particles within the conductive-dielectric object being imaged. Coil noise on the other hand is attributed to resistive losses of conducting metal elements within the resonant RF system. This includes losses in resistive wires/strips, lumped capacitive and inductive elements, solder joints, pre-amplifiers, cables, cable traps etc. Then the total resistance is given by $R_{tot} = R_{sample} + R_{conductors}$. While $R_{conductors}$ represents the series resistance of various electrical components in

the PCA at a particular frequency of operation, sample noise resistance R_{sample} depends on the spatial distribution of the sample conductivity $\sigma(\mathbf{r})$ and the (virtual transmit) electric field $\mathbf{E}(\mathbf{r})$ induced in the sample, i.e. $R_{sample} \propto \boldsymbol{\Psi}$ (Eq. (A4)).

Accelerated imaging with PCA: Acquiring the MR signal in the parallel fashion increases the SNR by a factor proportional to $\sqrt{L}$. By employing a partially parallel imaging (PPI) technique, such as SENSE, the $\sqrt{L}$ gain in SNR can be traded for a shorter scan time. The corresponding loss in SNR has been quantified as [11]:

$$\frac{\mathrm{SNR}^{\mathrm{PPI}}}{\mathrm{SNR}^{\mathrm{full}}} = \frac{1}{g\sqrt{R}} \tag{A6}$$

$$g = \sqrt{[(\mathbf{B}^H\boldsymbol{\Psi}^{-1}\mathbf{B})^{-1}]_{qq}(\mathbf{B}^H\boldsymbol{\Psi}^{-1}\mathbf{B})_{qq}} \geqslant 1 \tag{A7}$$

where $\mathrm{SNR}^{\mathrm{PPI}}$ is the SNR obtained with PPI and $\mathrm{SNR}^{\mathrm{full}}$ denotes the SNR that would be obtained with full gradient encoding under identical imaging conditions. Eq. (A6) accounts for two distinct types of losses. The factor $\sqrt{R}$ signifies a reduction of signal averaging when the total number of k-space samples n_k is reduced by the factor R. From the perspective of reconstruction strategy or coil design there is little that can be done to prevent this loss. The geometry factor g on the other hand reflects the ability of the coil array to complement reduced gradient encoding and is thus related to the geometrical configuration of the PCA. The geometry factor can be minimized to $g \cong 1$ by making the coil sensitivities as orthogonal as possible. Typically, PCA designs yield favorable g values up to reduction factors R between three and four [36,37]. Beyond this threshold however, dramatic increases in g are observed even with optimized arrays. This seems to confer some degree of restriction on the possible spatial variations of coil sensitivity patterns, which are governed by the solutions of Maxwell's equations [38].

References

[1] S.M. Wright, M.P. McDougall, Single echo acquisition MRI using RF encoding, NMR Biomed., doi:10.1002/nbm.1399.

[2] Y. Zhu, C.J. Hardy, D.K. Sodickson, R.O. Giaquinto, C.L. Dumoulin, G. Kenwood, T. Niendorf, H. Lejay, C.A. McKenzie, M.A. Ohlinger, N.M. Rofsky, Highly parallel volumetric imaging with a 32-element RF coil array, Magn. Reson. Med. 52 (2004) 869–877.

[3] P.B. Roemer, W.A. Edelstein, C.E. Hayes, S.P. Souza, O.M. Mueller, The NMR phased array, Magn. Reson. Med. 16 (1990) 192–225.

[4] M. Hutchinson, U. Raff, Fast MRI data acquisition using multiple detectors, Magn. Reson. Med. 6 (1998) 87–91.

[5] D. Kwiat, S. Einav, A decoupled coil detector array for fast image acquisition in magnetic resonance imaging, Med. Phys. 18 (1991) 251–265.

[6] G. Adriany, P.F. Van de Moortele, J. Ritter, S. Moeller, E.J. Auerbach, C. Akgün, C.J. Snyder, T. Vaughan, K. Ugurbil, A geometrically adjustable 16-channel transmit/receive transmission line array for improved RF efficiency and parallel imaging performance at 7 Tesla, Magn. Reson. Med. 59 (2008) 590–597.

[7] M. Griswold, P.M. Jakob, M. Nittka, J.W. Goldfarb, A. Haase, Partially parallel imaging with localized sensitivities (PILS), Magn. Reson. Med. 44 (2000) 602–609.

[8] M. Griswold, P.M. Jakob, R.M. Heidemann, M. Nittka, V. Jellus, J. Wang, B. Kiefer, A. Haase, Generalized autocalibrating partially parallel acquisitions (GRAPPA), Magn. Reson. Med. 47 (2002) 1202–1210.

[9] W.E. Kyriakos, L.P. Panych, D.F. Kacher, C.F. Westin, S.M. Bao, R.V. Mulkern, F.A. Jolesz, Sensitivity profiles from an array of coils for encoding and reconstruction in parallel (SPACE RIP), Magn. Reson. Med. 44 (2000) 301–308.

[10] D.K. Sodickson, W.J. Manning, Simultaneous acquisition of spatial harmonics (SMASH): ultra-fast imaging with radiofrequency coil arrays, Magn. Reson. Med. 38 (1997) 591–603.

[11] K.P. Pruessmann, M. Weiger, M.B. Scheidegger, P. Boesiger, SENSE: sensitivity encoding for fast MRI, Magn. Reson. Med. 42 (1999) 952–962.

[12] U. Katscher, P. Boernert, C. Leussler, J.S. van den Brink, Transmit SENSE, Magn. Reson. Med. 49 (2003) 144–150.

[13] J. Pauly, D. Nishimura, A. Macovski, A *k*-space analysis of small-tip angle excitation, J. Magn. Reson. 81 (1989) 43–56.

[14] G.J. Metzger, C. Snyder, C. Akgun, T. Vaughan, K. Ugurbil, P.F. Van de Moortele, Local B_1^+ shimming for prostate imaging with transceiver arrays at 7 T based on subject-dependent transmit phase measurements, Magn. Reson. Med. 59 (2008) 396–409.

[15] C.J. Hardy, H.E. Cline, R.O. Giaquinto, T. Niendorf, A.K. Grant, D.K. Sodickson, 32-Element receiver-coil array for cardiac imaging, Magn. Reson. Med. 55 (2006) 1142–1149.

[16] M.P. McDougall, S.M. Wright, 64-Channel array coil for single echo acquisition magnetic resonance imaging, Magn. Reson. Med. 54 (2005) 386–392.

[17] M. Schmitt, A. Potthast, D.E. Sosnovik, J.R. Polimeni, G.C. Wiggins, C. Triantafyllou, L.L. Wald, A 128-channel receive-only cardiac coil for highly accelerated cardiac MRI at 3 Tesla, Magn. Reson. Med. 59 (2008) 1431–1439.

[18] A. Trakic, B.K. Li, E. Weber, H. Wang, S. Wilson, S. Crozier, A rapidly rotating RF coil for MRI, Concepts Magn. Reson. B 35B (2009) 59–66.

[19] A. Trakic, B.K. Li, E. Weber, F. Liu, S. Wilson and S. Crozier, A mechanically rotating transceive system and method for applications in magnetic resonance, in: International Society for Magnetic Resonance in Medicine — 17th Scientific Meeting & Exhibition, Honolulu (Hawaii), April 2009.

[20] A. Trakic, B.K. Li, E. Weber, H. Wang, S. Wilson and S. Crozier, MRI with a rapidly rotating RF head coil, in: International Society for Magnetic Resonance in Medicine — 17th Scientific Meeting & Exhibition, Honolulu (Hawaii), April 2009.

[21] H.P.E. Stern, S.A. Mahmoud, Communication Systems: Analysis and Design, Prentice Hall, 2004.

[22] A. Haase, J. Frahm, D. Matthaei, W. Hinicke, K.D. Merboldt, FLASH imaging: rapid NMR imaging using low flip angle pulses, J. Magn. Reson. 67 (1986) 258–266.

[23] B.K. Li, E. Weber, F. Liu, S. Crozier, Hybrid MoM/FEM method for use in MRI, in: 29th Ann. Inter. Conf. IEEE Eng. Med. Biol. Society, 2007, pp. 3989.

[24] N. Tesla, Bladeless Turbine, U.S. Patents 1,061,206, 1911.

[25] P. Ullmann, S. Junge, M. Wick, F. Seifert, W. Ruhm, J. Hennig, Experimental analysis of parallel excitation using dedicated coil setups and simultaneous RF transmission on multiple channels, Magn. Reson. Med. 54 (2005) 994–1001.

[26] W.H. Press, B.P. Flannery, S.A. Teukolsky, W.T. Vetterling, Numerical Recipes in C: The Art of Scientific Computing, second ed., Cambridge University Press, 1992.

[27] K.P. Pruessmann, M. Weiger, P. Boernert, P. Boesiger, Advances in sensitivity encoding with arbitrary *k*-space trajectories, Magn. Reson. Med. 46 (2001) 638–651.

[28] B.E. Coggins, P. Zhou, Polar Fourier transforms of radially sampled NMR data, J. Magn. Reson. 182 (2006) 84–95.

[29] N. Seiberlich, F.A. Breuer, M. Blaimer, K. Barkauskas, P.M. Jakob, M.A. Griswold, Non-cartesian data reconstruction using GRAPPA operator gridding (GROG), Magn. Reson. Med. 58 (2007) 1257–1265.

[30] D. Hoult, Rotating frame zeugmatography, Philos. Trans. R. Soc. London, Ser. B. 289 (1980) 543–547.

[31] Nakanishi Inc., Tochigi, Japan. 2008. HTS1501S. Available from: <http://www.nsk-nakanishi.co.jp/industrial/home/>. Accessed on 5 September 2008.

[32] R.F. Lee, R.O. Giauinto, C.J. Hardy, Coupling and decoupling theory and its application to the MRI phased array, Magn. Reson. Med. 48 (2002) 203–213.

[33] M.A. Ohliger, P. Ledden, C.A. McKenzie, D.K. Sodickson, Effects of inductive coupling on parallel MR image reconstructions, Magn. Reson. Med. 52 (2004) 628–639.

[34] G.C. Wiggins, J.R. Polimeni, A. Potthast, M. Schmitt, V. Alagappan, L.L. Wald, 96-Channel receive-only head coil for 3 Tesla: design, optimization and evaluation, Magn. Reson. Med. 62 (2009) 754–762.

[35] A. Kumar, W.A. Edelstein, P.A. Bottomley, Noise figure limits for circular loop MR coils, Magn. Reson. Med. 61 (2009) 1201–1209.

[36] M. Weiger, K.P. Pruessmann, C. Leussler, P. Roschmann, P. Boesiger, Specific coil design for SENSE: a six element cardiac array, Magn. Reson. Med. 45 (2001) 495–504.

[37] J.A. de Zwart, P.J. Ledden, P. Kellman, P. van Gelderen, J.H. Duyn, Design of a SENSE-optimized high-sensitivity MRI receive coil for brain imaging, Magn. Reson. Med. 47 (2002) 1218–1227.

[38] F. Wiesinger, P. Boesiger, K.P. Pruessmann, Electrodynamics and ultimate SNR in parallel MR imaging, Magn. Reson. Med. 52 (2004) 376–390.